Fabrication and tribological characterization of laser textured boron cast iron surfaces

Xu, Yufu; Peng, Yubin; Dearn, Karl; You, Tao; Geng, Jian; Hu, Xianguo

DOI:
10.1016/j.surfcoat.2017.02.005

Document Version
Peer reviewed version

Citation for published version (Harvard):
Xu, Y, Peng, Y, Dearn, K, You, T, Geng, J & Hu, X 2017, 'Fabrication and tribological characterization of laser textured boron cast iron surfaces', *Surface and Coatings Technology*, vol. 313, pp. 391-401. https://doi.org/10.1016/j.surfcoat.2017.02.005

Fabrication and tribological characterization of the laser textured boron cast iron surfaces

Yufu Xu, Yubin Peng, Karl D. Dearn, Tao You, Jian Geng, Xianguo Hu

PII: S0257-8972(17)30147-0
DOI: doi: 10.1016/j.surfcoat.2017.02.005
Reference: SCT 22101

To appear in: *Surface & Coatings Technology*

Received date: 21 November 2016
Revised date: 1 February 2017
Accepted date: 2 February 2017

Please cite this article as: Yufu Xu, Yubin Peng, Karl D. Dearn, Tao You, Jian Geng, Xianguo Hu , Fabrication and tribological characterization of the laser textured boron cast iron surfaces. The address for the corresponding author was captured as affiliation for all authors. Please check if appropriate. Sct(2017), doi: 10.1016/j.surfcoat.2017.02.005

Fabrication and tribological characterization of the laser textured boron cast iron surfaces

Yufu Xu[a*], Yubin Peng[a], Karl D. Dearn[b], Tao You[a], Jian Geng[a], Xianguo Hu[a]

a. Institute of Tribology, School of Mechanical Engineering, Hefei University of Technology, Hefei 230009, China

b. School of Mechanical Engineering, University of Birmingham, Edgbaston, Birmingham B152TT, United Kingdom

[*] Corresponding author. Tel.: +86 551 62901359; fax: +86 551 62901359.

E-mail: xuyufu@hfut.edu.cn

Abstract: Laser surface texturing technology was employed for fabricating textured structures on cylinder liners. The tribological behaviour of the cylinder liners with different texturing structures including line, dimple and line + dimple and texturing area ratio was investigated under the lubrication of esterified bio-oil with and without MoS_2 microsheets as additives. The experimental results indicated that all the three textured surfaces showed better lubricating effects than untextured one except for the line + dimple structures leading to a higher wear rate to the cylinder liner; the dimple structures have better friction and wear performance than other structures. In addition, the textured surfaces lubricated with esterified bio-oil with MoS_2 microsheets presented the optimal friction reduction and antiwear properties. This might be ascribed to the fact that besides the adsorbed film composed of carbon and organics from the base oil, there was a robust complex composite tribo-film composed of MoS_2, MoO_3, FeOOH, FeO, Fe_2O_3, FeS, $FeSO_4$ and etc. on the rubbing surfaces. Furthermore, the dimples acted as an oil reservoir and provided a sink to pull wear debris away from the contacting surfaces. The combined actions of these factors gave rise to the lowest friction and wear of the tribopairs tested. The synergistic combination of the 12% area ratio dimples and MoS_2 microsheets showed great potential for application in IC engines, when coupled with bio-oil to reduce parasitic losses and energy consumption.

Key words: Cylinder liner; Piston ring; Laser surface texturing; MoS_2 microsheets; Boron cast iron surfaces

1. Introduction

In the pursuit of increased energy efficiency and an increasingly important requirement to reduce dependence on energy derived from fossil fuels, there is a growing corpus of research that seeks to both develop energy-saving technologies [1-4] and reliably harness renewable new energies [5]. This is no clearer than in Internal combustion engines, where, as an example, major efforts have been made to reduce frictional losses as an effective method to increase fuel efficiency. The tribological interaction between the Cylinder liner-piston ring (CLPR) forms the basis of the single most important friction pair in internal combustion (IC) engines, accounting for more than 50% of the frictional loss in an IC engine [6].

Laser surface texturing (LST) is a technology that has shown great potential for alleviating friction and wear of CLPR pairs [7-13]. Kligerman *et al.* [14] developed a partial LST on a piston ring set to improve tribological performance. They developed a theoretical model to optimize the texturing parameters, finding that the friction force was not affected by dimple diameter but decreased with an increasing texture area density. They found that frictional forces in textured CLPR were up to 30% lower than untextured piston rings. Guo *et al.* [10] reported significant differences in the friction and wear behavior of diesel simulated CLPR friction pairs with different surface texture structures. A concave texture was shown to provide the best antifriction and antiwear performance. Additionally, an appropriate depth-diameter ratio was shown to provide the optimum tribological combination. Hua *et al.* [9] found that using LST on the cylinder liner decreased oil

consumption by 45.5% , compared with a standard honed liner, due to the improved lubrication conditions.

Using lubricating additives is another important method to enhance the tribological performance of CLPR pairs. Among them molybdenum disulfide (MoS_2) nano-additives have been shown to provide excellent friction-reducing and antiwear properties. Sgroi *et al.* [15] dispersed inorganic fullerenes structures MoS_2 (IF-MoS_2) nanoparticles in an SAE 5W30 engine oil and reported a 50% reduction in friction coefficient under simulated diesel engine conditions. Demas *et al.* [16] reported that MoS_2 nanoparticles (nominal size 50 nm) significantly reduced both friction and wear of CLPR pairs, compared with a base oil. Raman spectra indicated that MoS_2 nanoparticles in the oil formed an aligned MoS_2 tribo-film resulting in a lower friction coefficient and reduced wear in the tribological samples.

It seems reasonable to assume, based on the above, that there may be some synergy when combining laser surface textures and lubricating additives, to further improve the tribological performance at the CLPR interaction, especially for the bio-oil lubricated conditions. However, little work has covered this area.

In this paper the results of an investigation in to the iterations between LST and a lubricant additive are reported. The tribological properties of three textures applied as a dimple, on the liner and on the ring are compared against a control. Due to the high cost of the nano-MoS_2 and the difficulties that are encountered when dispersing it in a base oil, commercially available MoS_2 microsheets were used as the lubricating additives. Esterified

bio-oil, a potentially effective renewable fuel, was used as the base oil for the lubricating additives [17]. Therefore, tests were also conducted to assess the magnitude of the effect of the lubrication additives working synergistically with the LST.

2. Experimental

2.1 Materials

Boron cast iron cylinder liners were supplied by Kaishan Cylinder Co. Ltd, China, and ductile iron piston rings were purchased from the Nanjing Feiyan Piston Ring Co., Ltd, China. Samples were cut to the following dimensions: liner -122 x 15.6 x 6.3 mm and piston ring 8 x 2 x 4 mm, to fit the tribometer. The liners were supplied without surface treatment and with a surface roughness (Ra) of 0.30 μm. The piston rings were received with a surface roughness of 0.25 μm. A detailed elemental analysis of the composition of the cylinder liner and the piston ring materials are shown in Table 1.

The MoS_2 micro sheets were bought from Shanghai chemical agents Ltd. Co., China. The size distribution, Raman spectra and powder X-ray diffraction (XRD) pattern of the MoS_2 are shown in **Fig. 1**. The results indicate that the mean size of the MoS_2 was 40.9 μm. Two characteristic peaks at 377 cm^{-1} and 403 cm^{-1} can be observed and are ascribed to the E_{2g}^1 and A_{1g} modes of MoS_2 [18]. In addition, the typical peaks of (002), (100), (103), (105) and (110) in the XRD pattern imply a crystalline structure to the MoS_2 microsheets [19]. According to the previous experimental results [20], the MoS_2 microsheets were dispersed in

the base oil with concentration of 1 wt.% using ultrasonic treatment for 15 min before tribological testing.

Esterified bio-oil was used as the base oil, which was synthesized via esterification of crude bio-oil derived from *Spirulina* algae with ethanol at 50 ^{o}C for 5 hours, using 5 wt.% KF/Al_2O_3 as a catalyst. The main components (peak area content) were as follows: esters 17.23%, ketones 5.28%, N-containing organics 14.97%, aldehydes 5.62%, alkanes 1.9%, and furan 3.03%. The basic properties of the esterified bio-oil are given in **Table 2**. More details of the esterification process, oil components and physical properties of the esterified bio-oil can be found in [17].

2.2 Laser surface texturing

The LST was carried out on an YLP-F10 fiber laser machine. A power of 5 W and a laser beam velocity of 300 mm/s was applied 10 times in the same area across the specimen. Line, dimple and line + dimple textures (LDT) were selected and fabricated into the surface of the liner samples. To facilitate additives and lubricating oil retension, both of the diameters of the line and dimple were about 1 mm, and the depth-to-diameter ratio was kept at 0.008 and 0.005 for dimple and line, respectively. The surface texturing area ratio (i.e. area of the textures/total area) was varied between 6%, 12% and 24%. Any bulge flash caused by the LST process was polished away with 3000# and 1200# metallographic abrasive paper. The textured surfaces were then ultrasonically treated in an acetone solution before the sliding tests. An optical microscope was employed to confirm the debris was

completely removed and to ensure that the bluges of samples were polished and the surface was suitable for the tribological tests. Examples of the texturing are shown in **Fig. 2.** The surface profile was measured using a Taylor Hobson surface profilometer. An enlarged image of a dimple and its profile are shown in **Fig. 3.** The widths and depths of the line and dimples were both about 1 mm and 8 μm, respectively. The interval between two dimples or lines was 3 mm.

2.3 Tribological tests and characterization

The tribological experiments were performed on a bespoke multi-functional cylinder liner-piston ring tribometer. A photograph of the tribometer and the schematic diagram of the friction pairs are shown in **Fig. 4.** The experimental conditions are listed in **Table 3.** The friction coefficient was recorded automatically during the tests and repeated twice for each experiment to reduce the experimental errors. The wear rate of the cylinder liner was calculated from the formula: $R = (W_o\text{-}W_i)/(F\times S)$, where W_o is the weight of the cylinder liner/piston ring before sliding (grams), and *Wi* is the weight of the cylinder/the piston ring after sliding (grams), F is the normal load (N), and S is the sliding distance (m).

The experimental specimens were washed with acetone after the tribological tests. To investigate the friction and wear mechanisms, the worn surfaces were observed with a scanning electron microscope (SEM, JSM-6490LV, JEOL, Japan) and a field emission scanning electron microscope (FESEM, SU8020, Hitachi, Japan) and analyzed using a LabRam HR Evolution Raman spectrometer (Horiba Jobin Yvon, France) with a 532 nm

laser. The chemical valences of the typical elements on the rubbed surfaces were measured by an ESCALAB 250 X-ray photoelectron spectroscope (XPS, Thermo Scientific, USA) equipped with a hemispherical electron analyzer and a non-monochromatic Al Kα X-ray source (1486.6 eV).

3. Results and discussion

3.1 Influence of texture structures

Fig. 5. shows the effect of texturing on the friction coefficient and wear rate under the lubrication of the base oil. Compared with the untextured cylinder liners, the textures induced a lower friction coefficient, which is in good agreement with literature [21, 22]. Both the untextured and textured surfaces had a run-in stage followed by a steady-state wear region. In the steady state region, the dimpled textures had the lowest friction coefficient, which decreased by 22% compared to the untextured surfaces. For the LDT surfaces, the friction coefficient was between that of the line textured and dimple textured surfaces, but the wear rate for LDT was much higher than that of untextured surfaces. This can be explained by the distance between textures and the sharp corners of the square angle cause a stress concentration [23] inducing surface cracking, leading to higher rates of wear. The wear rate of the corresponding piston ring samples did not increase. Both the dimple textured cylinder liners and piston rings samples presented the lowest wear rates, being some 58% and 46% lower respectively, compared the untextured test pieces. Based on these results, the dimple texturing was selected for the lubrication additive studies.

The texturing area ratios of 12% and 24% are shown in **Fig. 6**, the 6% area ratio is shown in Fig. 2 (c) and the tribological behaviours of the these samples lubricated with esterified bio-oil are shown in **Fig. 7**. When the area ratio was increased from 6% to 12%, both of the friction coefficient and wear rate decreased. A further increase area ratio however, to 24%, increased the steady-state friction coefficient by 17%, when compared to a 12% ratio. There was a very large increase in the wear rates, amounting to some 120% increase for the cylinder liner and 55% for piston ring samples. Although there are no obvious stress concentrations, the high texturing area ratio is likely to result in fatigue wear [24] because of the small interval between the textures. Moreover, the high texturing area ratio also resulted in higher contact pressures that might have increased the friction and wear of the tribological pairs. The surface with the texturing area ratio of 12% had the best antifriction and antiwear properties and was chosen for the lubrication additive studies.

3.2 Influence of the MoS_2 microsheets

Fig. 8. presents the comparison of the friction coefficient and wear rate of the textured and untextured surfaces lubricated by esterified bio-oil with and without MoS_2 microsheets. It can be seen that with the addition of MoS_2 both of the friction coefficient and wear rate of the untextured and textured surfaces decreased. For the untextured surfaces, the steady-state friction coefficient decreased by 8%. For the textured surfaces, the friction coefficient decreased by 26% after using the MoS_2 microsheets. Similar trends were observed for the wear rates of the frictional pairs. These results indicate that texturing not only helped to

reduce friction and wear between the samples [25], but also magnified the beneficial lubricating effects of the MoS_2 microsheets.

It is evident from Fig. 8(b) that, although only the cylinder liner was textured, both specimens benefited from lower wear rates compared to the untextured frictional pairs. Due to the similar chemical components (**Table 1**) and the antifriction and antiwear performances of the cylinder liner and piston ring specimens, the worn surfaces of the cylinder liner specimens were selected for further surface analysis to further understand the resulting lubricating mechanisms.

3.3 Worn surfaces analysis

Fig. 9 shows the SEM images of the worn surfaces under different conditions. It can be observed that the untextured surfaces without MoS_2 lubrication (Fig. 9a) have many severe furrows, indicative of severe wear. With the addition of the MoS_2 microsheets, wear severity was reduced to some light furrows and a few wear pits (Fig. 9b). This suggests that the introduction of the MoS_2 microsheets to the esterified bio-oil reduced both friction and wear. For the textured cylinder liners, irregular dimples and some cracks can be seen on the worn surfaces without MoS_2 lubrication (Fig. 9c). The dimples will have distorted due to deformation during the frictional process [26]. This distortion was reduced after adding the MoS_2 microsheets, as there was little change in the geometry of the dimples and no clear cracks on the worn surfaces (Fig. 9d). These results agree well with those in Fig. 8.

The Raman spectra from the worn surfaces are shown in **Fig. 10**. There are four wide peaks between 1250 and 1750 cm^{-1} under all conditions, indicating that an adsorbed film was formed on the rubbing surface [13]. For the untextured surfaces (Fig. 10a), the peak located at 790 cm^{-1} might be associated with iron oxides [27]. The intensity of this peak increased with the addition of MoS_2 microsheets, suggesting an increase of the oxide film on surface. Moreover, some peaks at 198, 282, 481, 564 and 944 cm^{-1} occurred on the worn untextured surfaces (Fig. 10b), which might be attributed to molybdenum oxide or sulfate [28]. If this is the case then the MoS_2 will have reacted with the components in the base oil and formed a tribo-film during the sliding process. In addition to the oxide or sulfate peaks, there are two typical MoS_2 peaks at 376 and 403 cm^{-1}, both detected on the textured surfaces with MoS_2 microsheets (Fig. 10d). The traces of MoS_2 detected on the rubbed surfaces suggest that the lubricating film formed might be more complex than that of untextured surfaces.

Raman spectra of the wide peaks, which are indicative of the adsorbed film, between 1250 to 1750 cm^{-1} in Fig. 10 were analyzed in **Fig. 11**. These peaks are likely to be the result of the carbonisation of the lubricating oil due to the local high temperature during the sliding [29]. Multi-Peaks Gaussian Fitting was used to deconvolve Raman spectra. The curves can be divided into two main peaks: D and G. The I_D/I_G ratio reflects the degree of graphitization, and the low I_D/I_G ratio suggests a high level graphitisation [30], which would help to reduce friction and wear. Comparing with the untextured surfaces (Fig. 11a, b), the textured ones (Fig. 11c, d) have a lower I_D/I_G ratio. This implies that the textured surfaces were covered

with an adsorbed film containing carbon with a higher degree of graphitization. This will have contributed to the better lubricating performance of the textured surfaces. In addition, with the introduction of MoS_2, the I_D/I_G ratios of both the untextured and textured surfaces decreased. The presence of MoS_2 was beneficial, facilitating the deposition of a carbon based tribo-film, which was good for lubrication.

The typical chemical elements on the rubbed surfaces were also analyzed by XPS, and the results of Fe2p are shown in **Fig. 12.** Multi-Peaks Gaussian Fitting was also employed to deconvolve XPS spectra. There are two typical Fe2p3/2 and Fe2p1/2 peaks detected on the surfaces tested for all of the frictional conditions. For the untextured surfaces, the peaks positioned at 709.09 (709.49) eV and 722.69 (722.53) eV belonged to the –Fe(II)–O– of FeO [31]; while the peaks at 710.63 (710.94) and 724.67 (724.96) eV are attributed to the –Fe(III)–O– of Fe_2O_3 [32]. These results indicated that a similar oxide film was formed on the rubbing surfaces. Moreover, a higher peak area ratio of Fe_2O_3 can be seen after adding MoS_2 microsheets. This suggests that with the introduction of MoS_2 a stable and robust oxide film was formed, resulting in better lubricating properties for the untextured surfaces after the introduction of the MoS_2 into the lubricating oil. These results are consistent with those in the Raman spectra. For the textured surfaces, the components of the oxide film were somewhat different. The peaks of FeO were detected, but the peaks at 711.25 (711.2) and 724.78 (724.43) eV could be ascribed to the –Fe(III)–O– of FeOOH [33], indicative of new species in the lubricating film. Furthermore, with the introduction of MoS_2, the new peaks at 713.49 and 725.72 eV could be ascribed to –Fe(II)–S– of FeS or $FeSO_4$, which promotes

antifriction and antiwear properties [34]. A more effective tribo-film was formed on the textured surfaces.

The C1 XPS spectra shown in **Fig. 13** give more information of the adsorbed organic components. For all of the experimental conditions, each main peak can be divided by three small peaks at ~284.67, ~286.11 and ~287.69 eV, ascribed to C-C/H, C-OH and C-COOR, respectively [35]. All of these are likely to have been derived from the hydrocarbons within the esterified bio-oil, i.e. carbon chains, alcohols and esters. With the same measurement conditions, the relative peak area can reflect the relative thickness of the adsorbed film. Thus, the textured surfaces had thicker adsorbed films than the untextured surfaces. This is to be expected as the textured dimples served as an oil reservoir under boundary lubrication conditions [36]. For the untextured surfaces, the introduction of MoS_2 seems to have had no significant effects on the amount of adsorbed organics on the surfaces, but clearly increased the concentration of alcohol organics, which may have been helpful to reduce friction and wear due to the excellent adsorbed abilities of the hydroxyl groups [37]. For the textured surfaces, the introduction of MoS_2 resulted in a little higher concentration of alcohols and esters in the tribo-film, which also contributed to improving the tribological performances of the tribosystem.

As shown in **Fig. 14** (a, b), the typical characteristic peaks of Mo3d and S2p were found on both the textured and untextured surfaces lubricated by base oil with MoS_2 microsheets. There were no obvious peaks at the same binding energy detected on the surfaces of samples lubricated with base oil but without MoS_2. This implies that the MoS_2

microsheets in the base oil are transferred to the surfaces during the sliding. To investigate the detailed composition of the tribo-film, the Mo3d and S2p peaks were divided and are shown in Fig. 14(c-f). For the untextured surfaces, the peak at 225.78 eV in Fig. 14 (c) is ascribed to S2s; the peaks at 229.07 and 232.36 eV belong to Mo3d5/2 and Mo3d3/2 of –Mo(IV)–S– in MoS_2 [38], indicating that some MoS_2 remained on the surfaces as a result of deformation. This seems to be contrast to the Raman spectra in Fig.10b since no obvious MoS_2 peaks were detected. This might be because of a very low concentration of MoS_2 on the worn surfaces and so it is hard detected using Raman spectra, but can be measured by XPS with a higher resolution. The peaks positioned at 233.65 and 235.64 eV are attributed to Mo3d5/2 and Mo3d3/2 of –Mo(VI)–S– in MoO_3 [39], suggesting some oxide components in the tribo-film are formed. In addition to this, the peaks at 161.81 and 163 eV in Fig. 14 (d) indicate that some sulfides such as FeS and MoS_2 might be present on the worn untextured surfaces. This corroborates the results given of Mo3d in Fig. 14 (c) but do not agree with those of Fe2p spectra in Fig. 12 since there were no obvious peaks of FeS. This may again be a result of the resolution of the equipment.

For the textured surfaces, the concentrations of Mo and S are much higher than those on the untextured surfaces since they have bigger relative peak areas under the same measured conditions, suggesting that the tribo-film on the textured surface was much thicker than that on the untextured surface. There are also two new peaks at 167.73 and 168.26 eV shown in Fig. 14(f), which can be ascribed to S2p3/2 and S2p1/2 of –S(IV)–O–in $FeSO_4$.

This is consistent with the Fe2p results shown in Fig. 12. This provides further proof of the complexity of the tribo-film, relative to the untextured surfaces.

Based on the above, a schematic diagram of the lubricating mechanisms under different conditions is given in **Fig. 15**. For the untextured surface lubricated with base oil (Fig. 15a), an adsorbed film dominated the lubricating process, and it was composed of carbon and organics including hydrocarbons with carbon chains, alcohols and esters from the base oil. There was also a thin oxide tribo-film composed predominately of FeO and Fe_2O_3 on the substrate,. Due to the unstable properties of the oxide tribo-film, the rubbed surfaces presented a relative heavy wear (Fig. 9a). With the introduction of MoS_2 microsheets, a more stable oxide film was present, strengthened by a higher concentration of Fe_2O_3 and a thicker adsorbed film (Fig. 15b), leading to decreased friction and wear of the tribo-pairs.

For the textured surfaces lubricated with base oil (Fig. 15c), the dimples acted as an oil reservoir, leading to a thicker adsorbed film, and better lubricating performance.

When MoS_2 was added to the base oil (Fig. 15d), a stable and robust composite tribo-film including MoS_2, MoO_3, FeOOH, FeO, Fe_2O_3, FeS, $FeSO_4$ etc. was formed in addition to the adsorbed film described above, result in the lowest friction and wear.

4. Conclusions

This paper assessed the interactions between laser surface texturing and a lubricant additive leading to reduced friction and wear in simulated cylinder liner/ piston ring. The tribological properties of three textures applied on the liner sample were compared against a

control. A renewable base oil esterified bio-oil was chosen for the lubricating media and MoS_2 micro-sheets were used as the solid lubricating additives. The tribological tests were performed on a cylinder liner-piston ring tribometer and a variety of analytical equipment was used to discern the synergistic interactions between the physical and chemical measures taken to improve tribological performance. The following conclusions can be drawn from this work:

- All of the textured surfaces assessed including line, dimple, and line + dimple structures had a better tribological performance than untextured surfaces of cylinder liners. The only exception to this was the line + dimple structures which might lead to a higher wear rate to the cylinder liner, as a result of fatigue at the sharp edges of the textures.
- Among the investigated textures, the dimple geometry showed the best antifriction and antiwear properties. Friction levels decreased by 22% and wear rates by 58% and 46% for the cylinder liners and piston rings respectively, compared to those of untextured surfaces.
- Increasing the texture area ratio of the cylinder liners with dimples from 6% to 24% lead to mixed results, with the optimal friction and wear behavior at 12% textured area ratio under the tested conditions.
- For the untextured surfaces lubricated with the bio oil, the main lubricating film was composed of a thin oxide film and a larger adsorbed film including carbon and organics from esterified bio-oil. When MoS_2 microsheets were added, both the

oxide film and the adsorbed film became thicker. There was also a new tribo-film composed of FeS and MoO_3 formed leading to better lubricating performance.

- For the textured surfaces lubricated with the bio oil, the dimples provided a debris absorbing function and led to a dynamic adsorbed film. When MoS_2 microsheets were added, a robust composite tribo-film composed of MoS_2, MoO_3, FeOOH, FeO, Fe_2O_3, FeS and $FeSO_4$ was formed. When coupled with the adsorbed film seen in the other tests, the composite film led to the best tribological performance, showing great potential for application in IC engines to reduce parasitic losses and reduce energy consumption.

Acknowledgments

The authors appreciate and acknowledge the assistance of Ms. Fangyuan Wu in developing the texturing. This work was supported by the National Natural Science Foundation of China (Grant No. 51405124), China Postdoctoral Science Foundation (Grant Nos. 2015T80648 & 2014M560505) and the Tribology Science Fund of State Key Laboratory of Tribology, Tsinghua University (Grant No. SKLTKF15A05). Some of the experimental equipment used in this research, within the Birmingham Centre for Cryogenic Energy Storage, was obtained with support from the Engineering and Physical Sciences Research Council, under the eight great technologies: energy storage theme (Grant No. EP/L017725/1). The authors gratefully acknowledge the support of the China Scholarship

Council for facilitating Dr. Yufu Xu as a visiting scholar in Professor Wilfred T. Tysoe's group at UW Milwaukee, USA.

References:

[1] N.T. Kalyani, S. Dhoble, Organic light emitting diodes: energy saving lighting technology—a review, Renewable Sustainable Energy Rev., 16 (2012) 2696-2723.

[2] D. Zheng, Z.B. Cai, M.X. Shen, Z.Y. Li, M.H. Zhu, Investigation of the tribology behaviour of the graphene nanosheets as oil additives on textured alloy cast iron surface, Appl Surf Sci, 387 (2016) 66-75.

[3] S. Amini, H.N. Hosseinabadi, S.A. Sajjady, Experimental study on effect of micro textured surfaces generated by ultrasonic vibration assisted face turning on friction and wear performance, Appl Surf Sci, 390 (2016) 633-648.

[4] Q. Ma, F. Zhou, S. Gao, Z. Wu, Q. Wang, K. Chen, Z. Zhou, K.Y. Li, Influence of boron content on the microstructure and tribological properties of Cr-B-N coatings in water lubrication, Appl Surf Sci, 377 (2016) 394-405.

[5] F. Manzano-Agugliaro, A. Alcayde, F. Montoya, A. Zapata-Sierra, C. Gil, Scientific production of renewable energies worldwide: an overview, Renewable Sustainable Energy Rev., 18 (2013) 134-143.

[6] S. Johansson, P.H. Nilsson, R. Ohlsson, B.-G. Rosén, Experimental friction evaluation of cylinder liner/piston ring contact, Wear, 271 (2011) 625-633.

[7] E. Tomanik, Modelling the hydrodynamic support of cylinder bore and piston rings with laser textured surfaces, Tribol Int, 59 (2013) 90-96.

[8] W. Grabon, W. Koszela, P. Pawlus, S. Ochwat, Improving tribological behaviour of piston ring–cylinder liner frictional pair by liner surface texturing, Tribol Int, 61 (2013) 102-108.

[9] X. Hua, J. Sun, P. Zhang, H. Ge, F. Yonghong, J. Jinghu, B. Yin, Research on discriminating partition laser surface micro-texturing technology of engine cylinder, Tribol Int, 98 (2016) 190-196.

[10] Z. Guo, C. Yuan, P. Liu, Z. Peng, X. Yan, Study on Influence of Cylinder Liner Surface Texture on Lubrication Performance for Cylinder Liner–Piston Ring Components, Tribol Lett, 51 (2013) 9-23.

[11] Y. Zhou, H. Zhu, W. Tang, C. Ma, W. Zhang, Development of the theoretical model for the optimal design of surface texturing on cylinder liner, Tribol Int, 52 (2012) 1-6.

[12] A. Ahmed, H. Masjuki, M. Varman, M. Kalam, M. Habibullah, K. Al Mahmud, An overview of geometrical parameters of surface texturing for piston/cylinder assembly and mechanical seals, Meccanica, 51 (2016) 9-23.

[13] B. Yin, X. Li, Y. Fu, W. Yun, Effect of laser textured dimples on the lubrication performance of cylinder liner in diesel engine, Lubr. Sci., 24 (2012) 293-312.

[14] Y. Kligerman, I. Etsion, A. Shinkarenko, Improving Tribological Performance of Piston Rings by Partial Surface Texturing, J. Tribol., 127 (2005) 632-638.

[15] M. Sgroi, F. Gili, D. Mangherini, I. Lahouij, F. Dassenoy, I. Garcia, I. Odriozola, G. Kraft, Friction reduction benefits in valve-train system using IF-MoS_2 added engine oil, Tribol T, 58 (2015) 207-214.

[16] N.G. Demas, E.V. Timofeeva, J.L. Routbort, G.R. Fenske, Tribological effects of BN and MoS_2 nanoparticles added to polyalphaolefin oil in piston skirt/cylinder liner tests, Tribol Lett, 47 (2012) 91-102.

[17] Y. Xu, X. Zheng, X. Hu, K.D. Dearn, H. Xu, Effect of catalytic esterification on the friction and wear performance of bio-oil, Wear, 311 (2014) 93-100.

[18] Y. Xu, Y. Peng, K.D. Dearn, X. Zheng, L. Yao, X. Hu, Synergistic lubricating behaviors of graphene and MoS_2 dispersed in esterified bio-oil for steel/steel contact, Wear, 342 (2015) 297-309.

[19] K. Zhao, W. Gu, L. Zhao, C. Zhang, W. Peng, Y. Xian, MoS_2/nitrogen-doped graphene as efficient electrocatalyst for oxygen reduction reaction, Electrochim Acta, 169 (2015) 142-149.

[20] Z.Y. Xu, K.H. Hu, C.L. Han, X.G. Hu, Y.F. Xu, Morphological influence of molybdenum disulfide on the tribological properties of rapeseed oil, Tribol Lett, 49 (2013) 513-524.

[21] S.-C. Vlădescu, A.V. Olver, I.G. Pegg, T. Reddyhoff, Combined friction and wear reduction in a reciprocating contact through laser surface texturing, Wear, 358–359 (2016) 51-61.

[22] J. Hu, H. Xu, Friction and wear behavior analysis of the stainless steel surface fabricated by laser texturing underwater, Tribol Int, 102 (2016) 371-377.

[23] W.S. Zhang, X. Guo, M.Y. Wang, P. Wei, Optimal topology design of continuum structures with stress concentration alleviation via level set method, Int J Numer Meth Eng, 93 (2013) 942-959.

[24] Y. Wu, Y. Zhou, J. Li, H. Zhou, J. Chen, H. Zhao, A comparative study on wear behavior and mechanism of styrene butadiene rubber under dry and wet conditions, Wear, 356 (2016) 1-8.

[25] D. He, S. Zheng, J. Pu, G. Zhang, L. Hu, Improving tribological properties of titanium alloys by combining laser surface texturing and diamond-like carbon film, Tribol Int, 82 (2015) 20-27.

[26] S. Fatemi-Varzaneh, A. Zarei-Hanzaki, S. Izadi, Shear deformation and grain refinement during accumulative back extrusion of AZ31 magnesium alloy, J Mater Sci, 46 (2011) 1937-1944.

[27] R.Y. Ho, G. Roelfes, B.L. Feringa, L. Que, Raman evidence for a weakened OO bond in mononuclear low-spin iron (III)-hydroperoxides, J Am Chem Soc, 121 (1999) 264-265.

[28] G.W. Li, C.S. Li, H. Tang, K.S. Cao, J.A. Chen, F.F. Wang, Y. Jin, Synthesis and characterization of hollow MoS_2 microspheres grown from MoO_3 precursors, J Alloy Compd, 501 (2010) 275-281.

[29] X. Qi, Z. Jia, Y. Yang, B. Fan, Characterization and auto-restoration mechanism of nanoscale serpentine powder as lubricating oil additive under high temperature, Tribol Int, 44 (2011) 805-810.

[30] J.-T. Jiu, H. Wang, C.-B. Cao, H.-S. Zhu, The effect of annealing temperature on the structure of diamond-like carbon films by electrodeposition technique, J Mater Sci, 34 (1999) 5205-5209.

[31] W. Mi, H. Liu, Z. Li, P. Wu, E. Jiang, H. Bai, Evolution of structure, magnetic and transport properties of sputtered films from Fe to Fe_3O_4, J. Phys. D: Appl. Phys., 39 (2006) 5109.

[32] Y. Xu, Y. Peng, X. Zheng, H. Wang, X. Hu, Influence of microalgal bio-oil on the lubrication properties of engine oil, Oil Gas Sci. Technol., 71 (2016) 10.

[33] C. Gao, G. Zhang, T. Wang, Q. Wang, Enhancing the tribological performance of PEEK exposed to water-lubrication by filling goethite (α-FeOOH) nanoparticles, RSC Adv., 6 (2016) 51247-51256.

[34] J. Guan, X. Xu, W. Peng, Tribological properties of phenolic resin bonded abrasive tools filled with two inclusion complexes of β-cyclodextrin and sulfur-containing additives, Proceedings of the Institution of Mechanical Engineers, Part J: Journal of Engineering Tribology, 228 (2014) 725-734.

[35] H. Yu, J. He, L. Sun, S. Tanaka, B. Fugetsu, Influence of the electrochemical reduction process on the performance of graphene-based capacitors, Carbon, 51 (2013) 94-101.

[36] D. Xiong, Y. Qin, J. Li, Y. Wan, R. Tyagi, Tribological properties of PTFE/laser surface textured stainless steel under starved oil lubrication, Tribol Int, 82 (2015) 305-310.

[37] J. Qiu, G. Wang, Y. Bao, D. Zeng, Y. Chen, Effect of oxidative modification of coal tar pitch-based mesoporous activated carbon on the adsorption of benzothiophene and dibenzothiophene, Fuel Process Technol, 129 (2015) 85-90.

[38] W. Yang, Q.-Q. Sun, Y. Geng, L. Chen, P. Zhou, S.-J. Ding, D.W. Zhang, The integration of sub-10 nm gate oxide on MoS_2 with ultra low leakage and enhanced mobility, Sci. Rep., 5 (2015).

[39] M. JF, W. Stickle, S. PE, B. KD, Handbook of X-ray photoelectron spectroscopy, Phys. Electronics Inc, Eden Prairie, 1995.

Table 1 Chemical components of the cylinder liner and piston ring specimens

Components /wt. %	C	Si	P	Mn	B	Cr	Mg	Fe
Cylinder liner	3.22	2.33	0.25	0.81	0.05	0.36	-	Balanced
Piston ring	3.55	2.72	<0.08	<0.5	-	-	0.03	Balanced

Table 2 Properties of the esterified bio-oil

Parameters	Values
C/wt%	45.49
H/wt%	8.57
N/wt%	0.97
O*/wt%	44.97
Frozen point/^{o}C	<-58
Density/kg m^{-3}	866.25
Viscosity at 40 ^{o}C /mm^{2} s^{-1}	1.34

* By difference

Table 3 Tribological testing conditions

Testing conditions	Value
Reciprocating frequency / Hz	5
Stroke / mm	80
Testing temperature / ^{o}C	90
Oil feed rate / mL·h^{-1}	20
Sliding velocity / m·s^{-1}	0.8
Normal Load / N	210
Duration / min	160

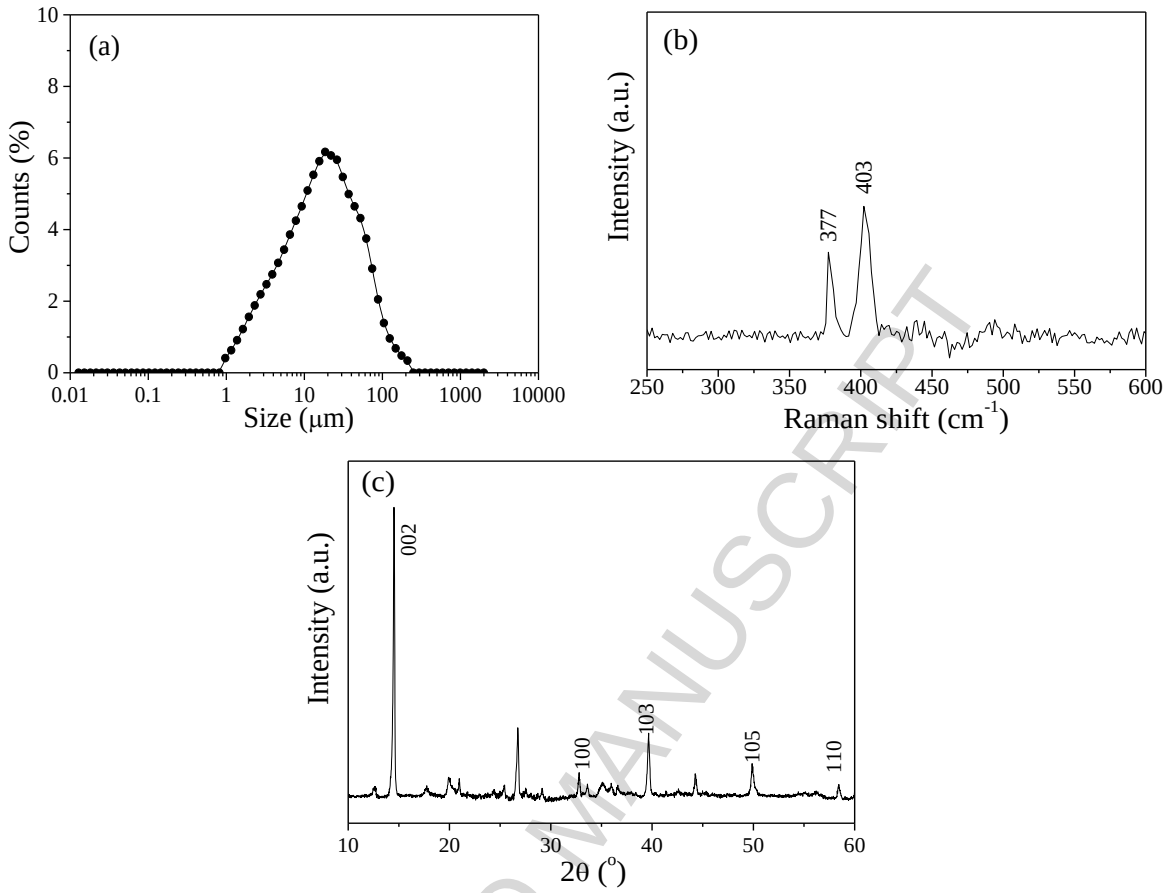

Fig. 1 Size distribution (a), Raman spectra (b) and XRD pattern (c) of MoS_2 microsheets

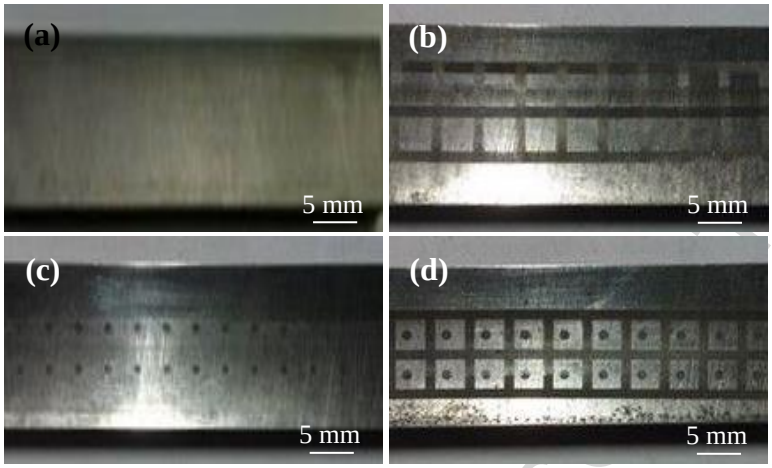

Fig. 2 Images of untextured (a) and textured surfaces: liners (b), dimples (c) and liners plus dimples (d)

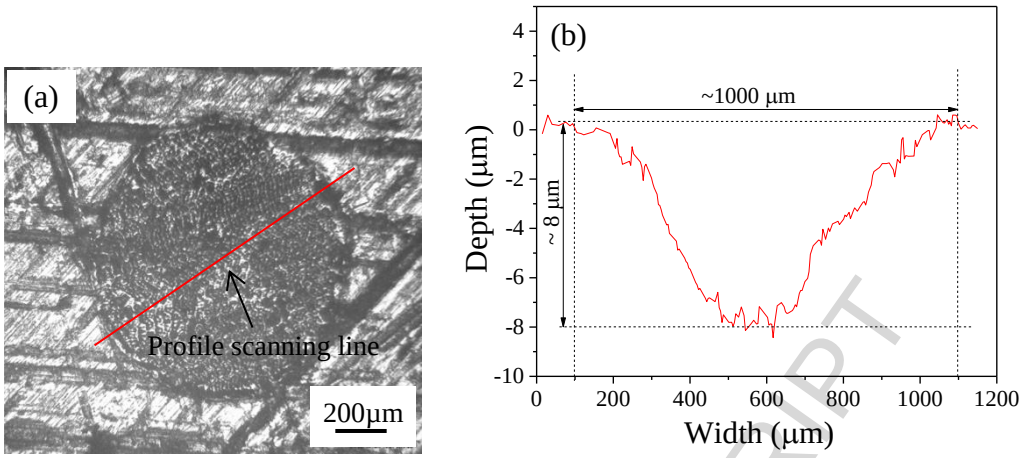

Fig. 3 Amplified images of single dimple (a) and its profile scanning curve (b)

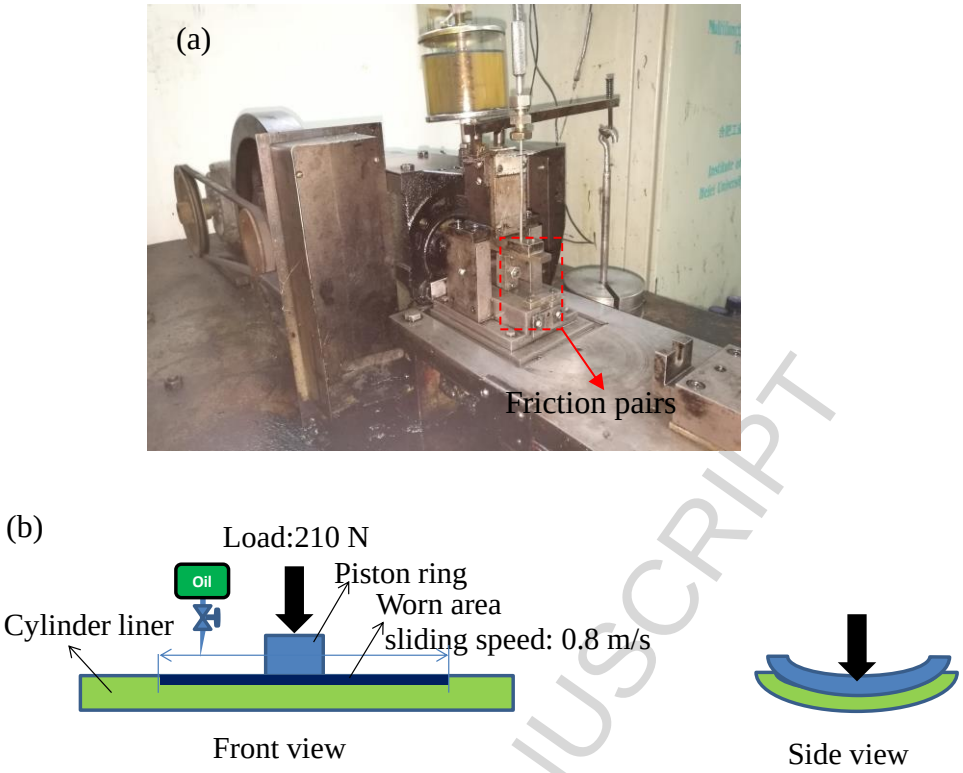

Fig. 4 A photograph (a) of the multi-functional cylinder liner–piston ring tribometer and the schematic (b) of the friction pairs

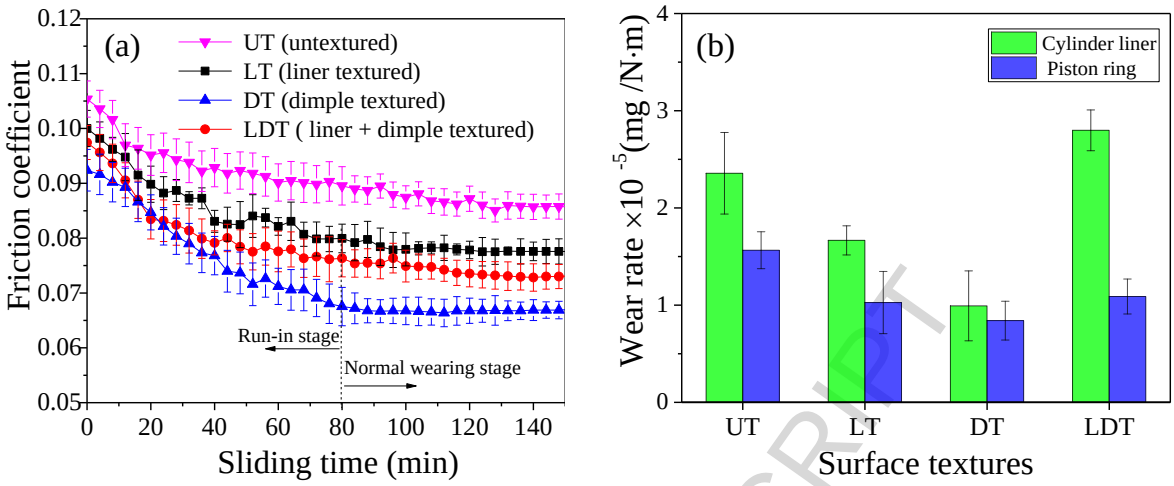

Fig. 5. Influence of texturing structures on the friction coefficient (a) and wear rate (b)

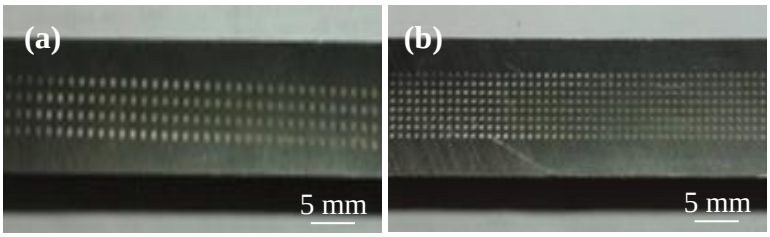

Fig. 6. Images of different texturing area ratio: (a) 12% and (b) 24%

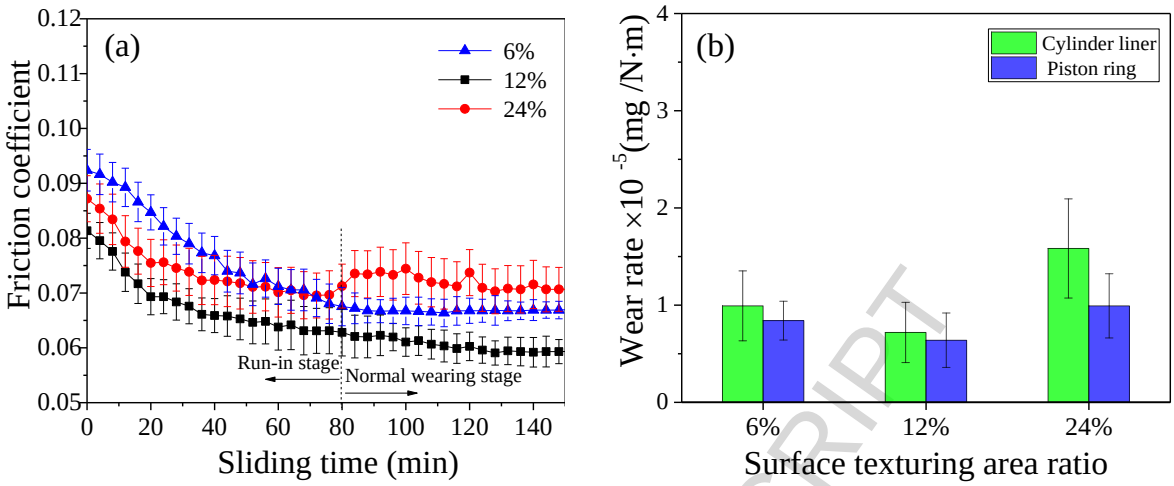

Fig. 7. Influence of texturing area ratio on the friction coefficient (a) and wear rate (b)

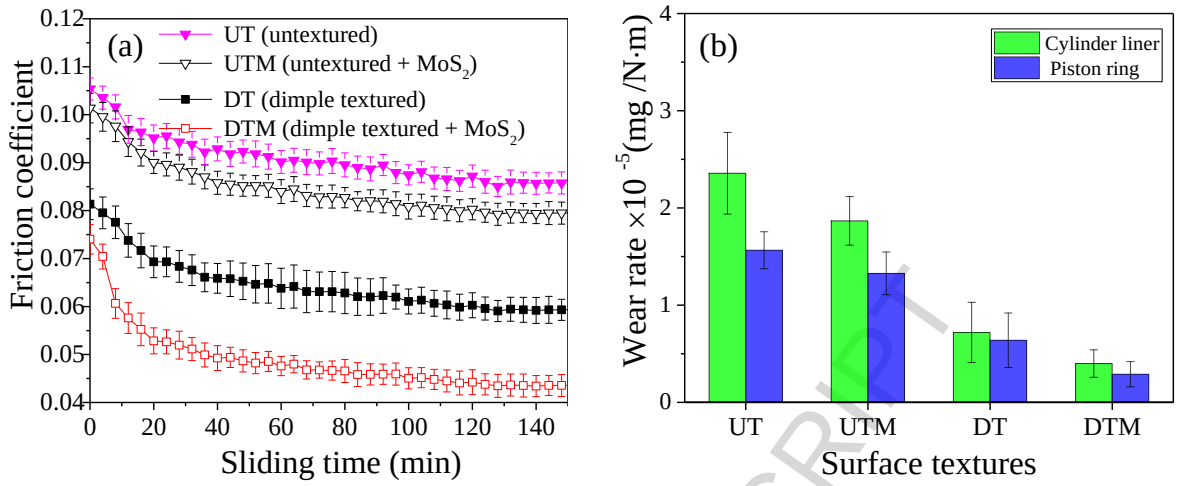

Fig. 8. Comparison of the friction coefficient (a) and wear rate (b) under the untextured and textured surfaces with or without MoS_2 microsheets

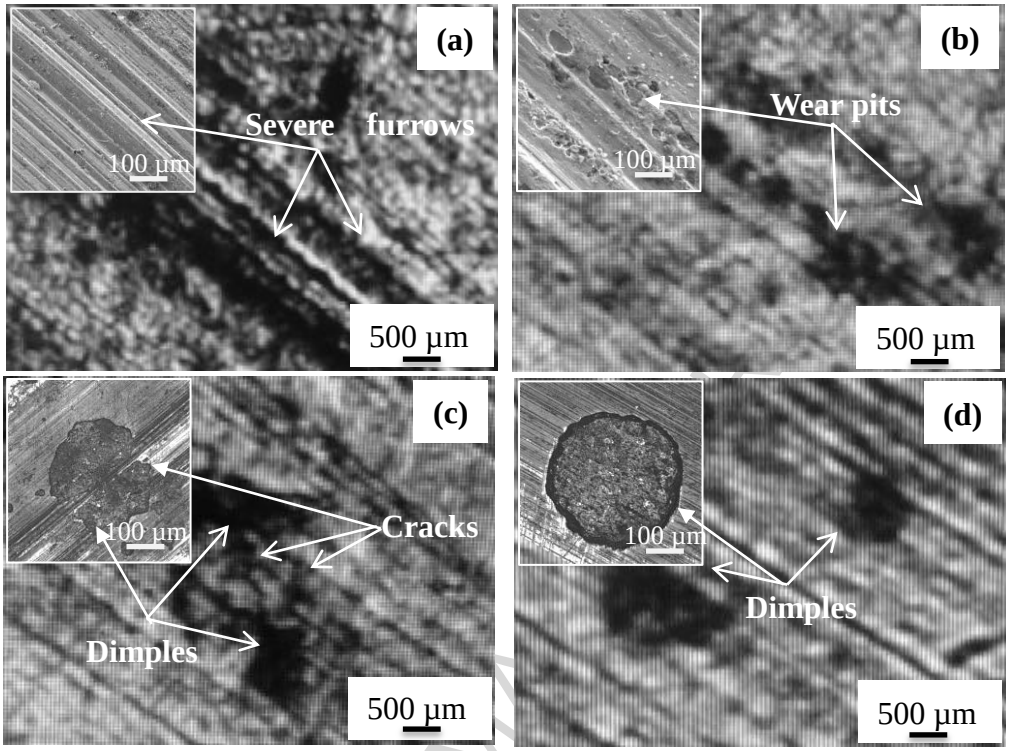

Fig. 9. SEM images (insets are partial enlarged detail with FESEM) of the worn untextured (a, b) and textured (c, d) surfaces with (b, d) or without (a, c) MoS_2 microsheets

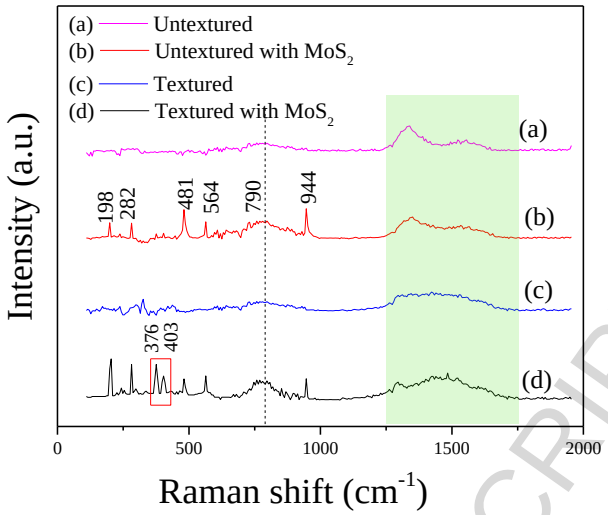

Fig. 10. Raman spectra on the worn surfaces under the untextured (a, b) and textured surfaces (c, d) with (b, d) or without MoS_2 microsheets (a, c)

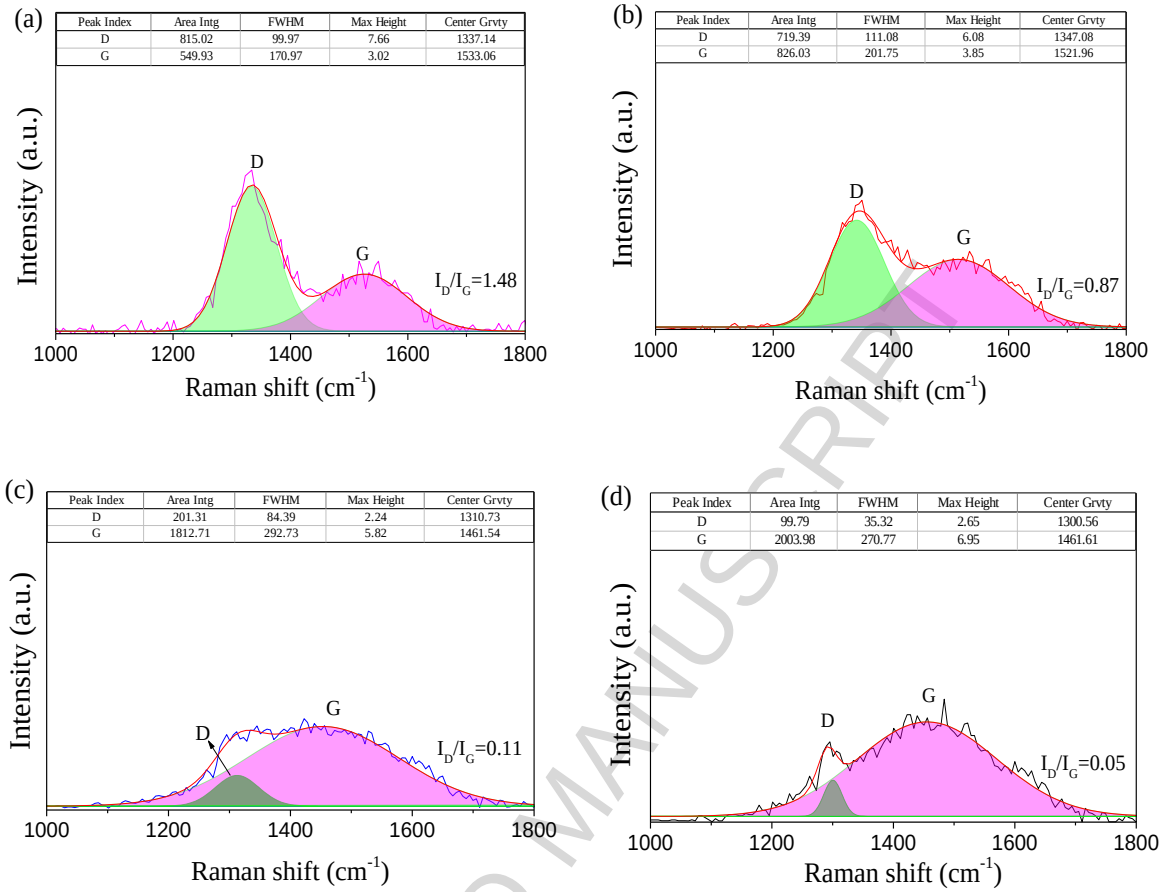

Fig. 11. Raman spectra of the carbon on the worn surfaces under the untextured (a, b) and textured (c, d) surfaces with (b, d) or without (a, c) MoS_2 microsheets

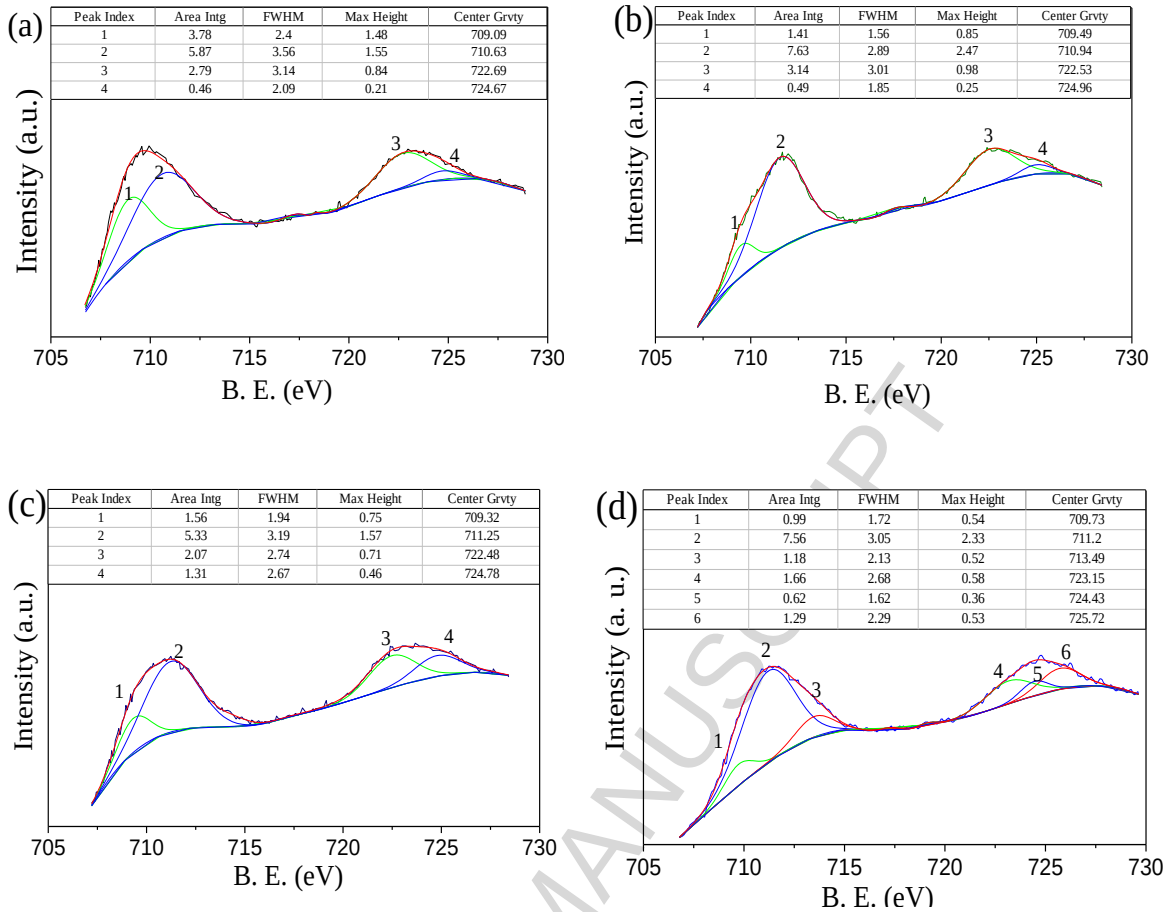

Fig. 12. XPS spectra of Fe2p on the worn surfaces under the untextured (a, b) and textured (c, d) surfaces with (b, d) or without (a, c) MoS_2 microsheets

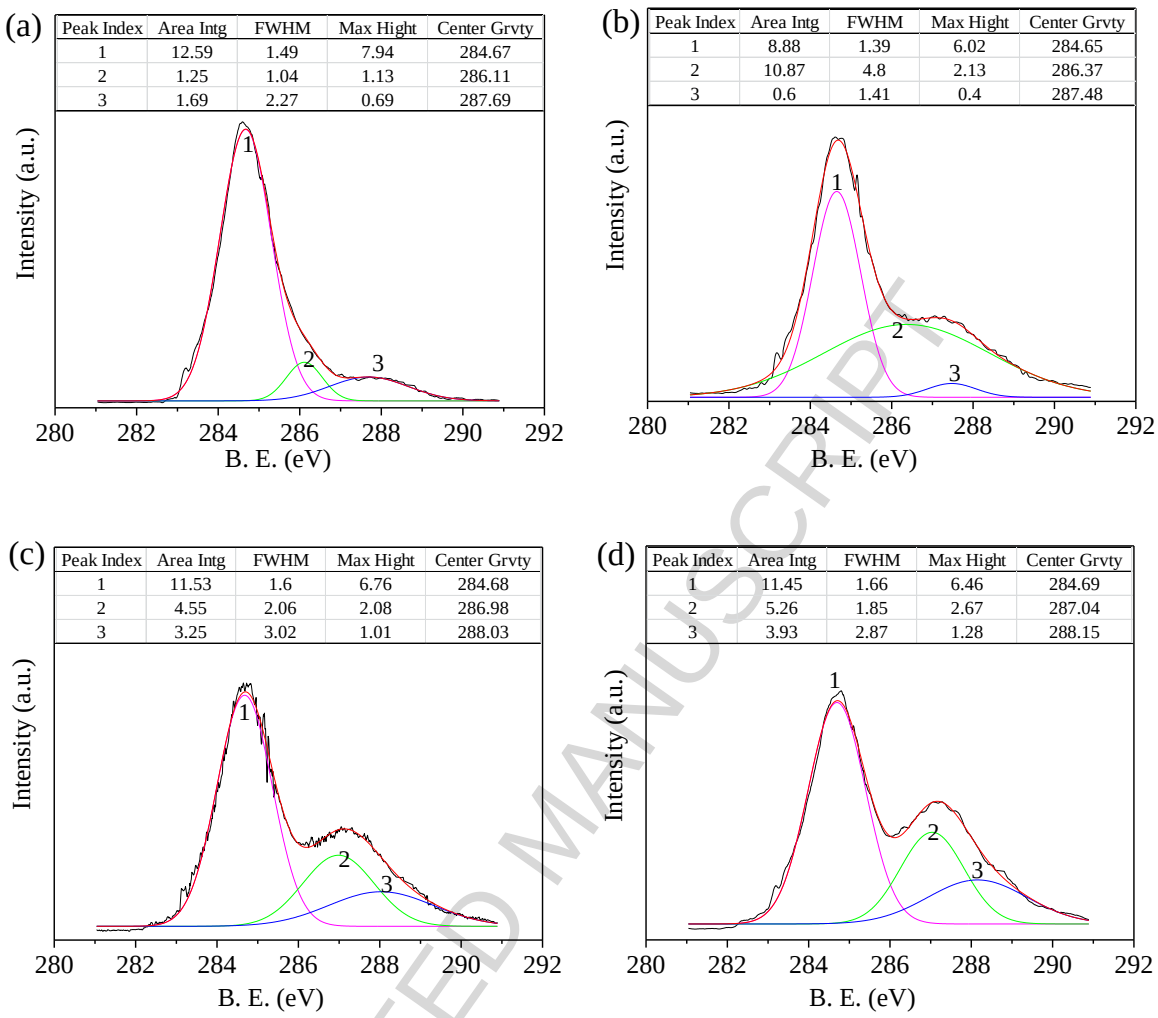

Fig. 13. XPS spectra of C1s on the worn surfaces under the untextured (a, b) and textured (c, d) surfaces with (b, d) or without (a, c) MoS_2 microsheets

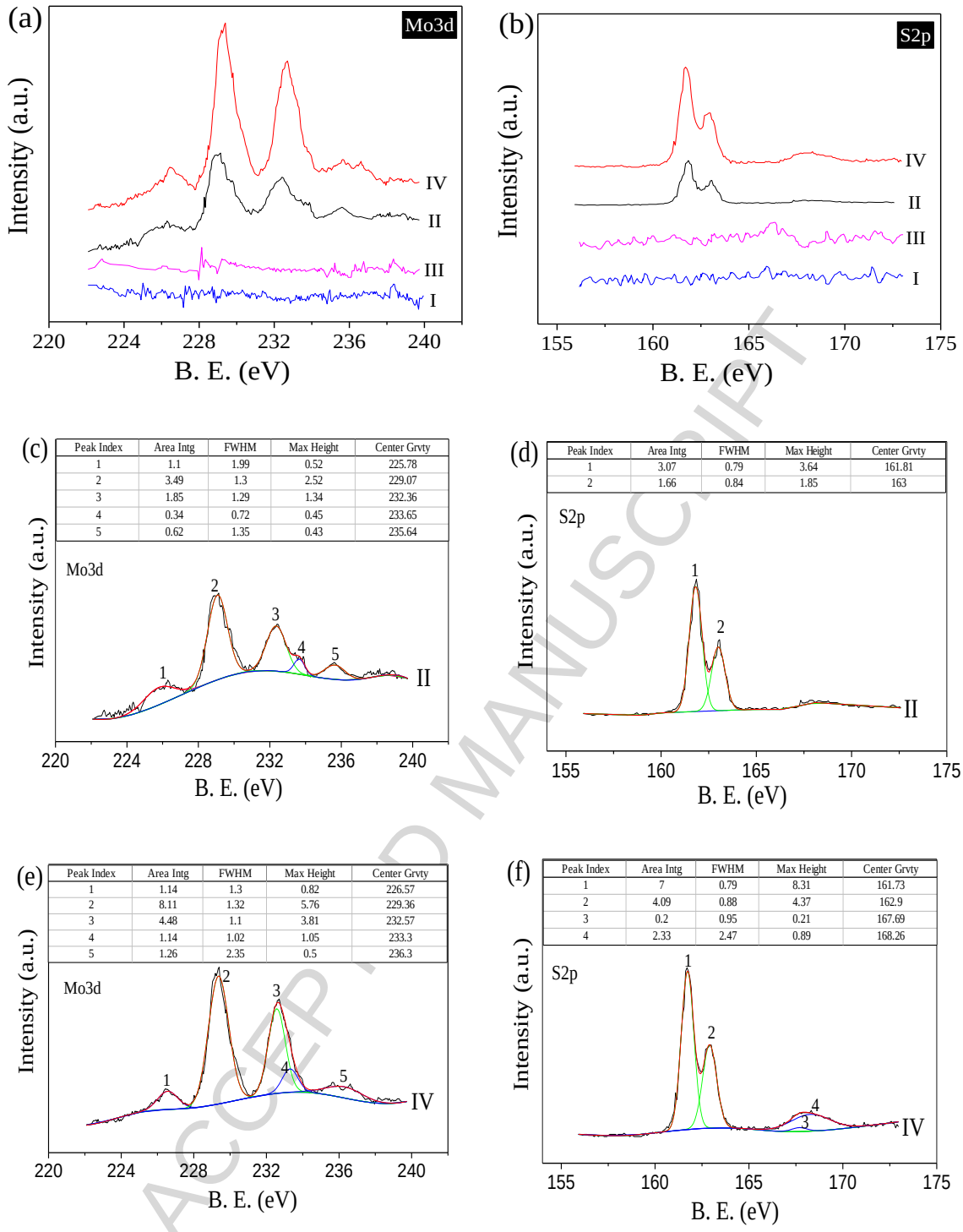

Fig. 14. XPS spectra of Mo3d (a, c, e) and S2p (b, d, f) on the worn surfaces under the untextured (I, II) and textured (III, IV) surfaces with (II, IV) or without (I, III) MoS_2 microsheets

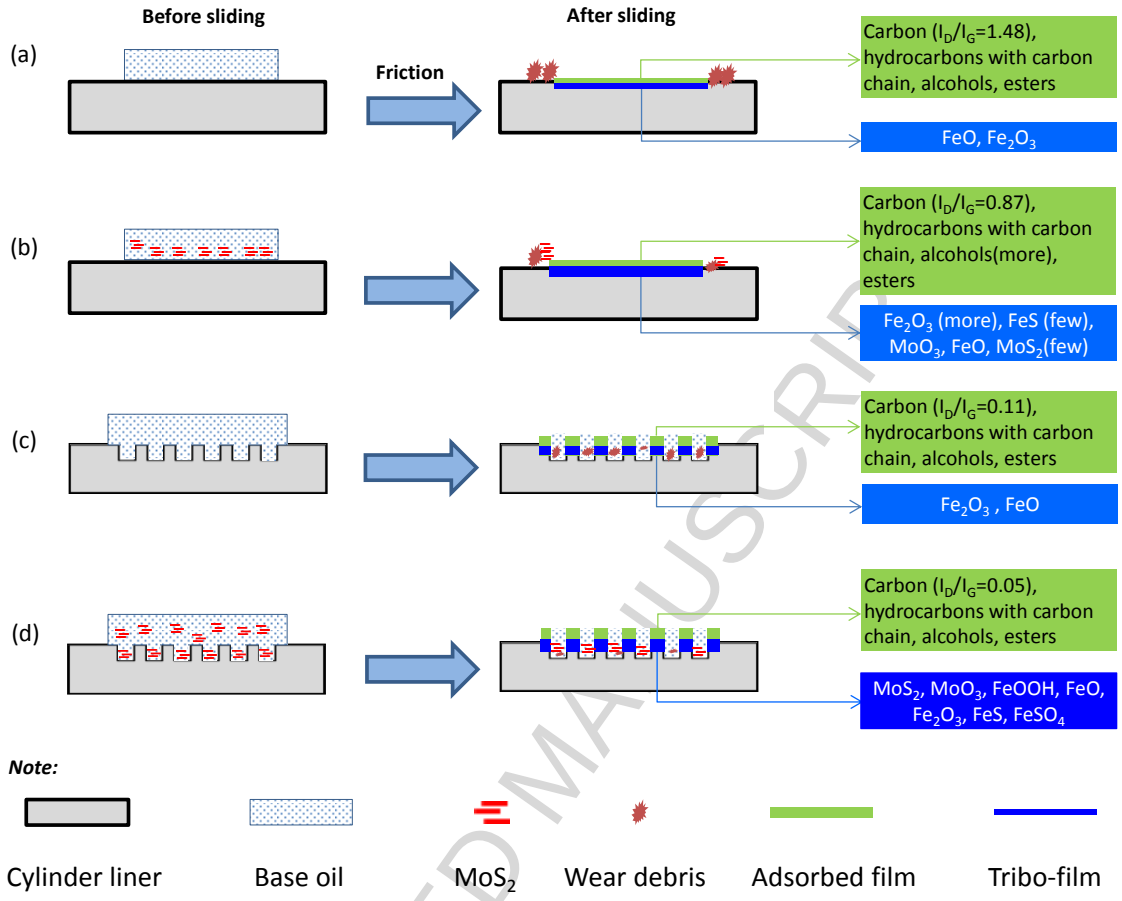

Fig. 15. Schematic explanation of the lubricating mechanisms under the untextured (a, b) and textured (c, d) surfaces with (b, d) or without (a, c) MoS_2 microsheets

Highlights

- Three typical micro-structure textured boron cast iron surfaces were fabricated.
- Friction and wear behaviors of the textured surfaces were investigated.
- The dimple microstructures show the optimal performances.
- Corresponding micro-mechanisms were illustrated.